

# Three-Dimensional Transport Model for Intravitreal and Suprachoroidal Drug Injection

Yu Zhang,<sup>1</sup> Hojjat Bazzazi,<sup>1</sup> Raquel Lima e Silva,<sup>2</sup> Niranjana B. Pandey,<sup>1</sup> Jordan J. Green,<sup>1,2</sup> Peter A. Campochiaro,<sup>2</sup> and Aleksander S. Popel<sup>1</sup>

<sup>1</sup>Department of Biomedical Engineering, School of Medicine, Johns Hopkins University, Baltimore, Maryland, United States

<sup>2</sup>Wilmer Eye Institute, School of Medicine, Johns Hopkins University, Baltimore, Maryland, United States

Correspondence: Yu Zhang, Department of Biomedical Engineering, School of Medicine, Johns Hopkins University, Baltimore, MD 21205, USA; zhangyu@jhmi.edu.

Submitted: April 1, 2018

Accepted: September 26, 2018

Citation: Zhang Y, Bazzazi H, Lima e Silva R, et al. Three-dimensional transport model for intravitreal and suprachoroidal drug injection. *Invest Ophthalmol Vis Sci.* 2018;59:5266-5276. <https://doi.org/10.1167/iovs.17-23632>

**PURPOSE.** Quantitative understanding of the transport of therapeutic macromolecules following intraocular injections is critical for the design of efficient strategies in treating eye diseases, such as neovascular (wet) age-related macular degeneration (AMD) and macular edema (ME). Antiangiogenic treatments, such as neutralizing antibodies against VEGF or recently characterized antiangiogenic peptides, have shown promise in slowing disease progression.

**METHODS.** We developed a comprehensive three-dimensional (3D) transport model for intraocular injections using published data on drug distribution in rabbit eyes following intravitreal and suprachoroidal (SC) injection of sodium fluorescein (SF), bevacizumab, and ranibizumab. The model then was applied to evaluate the distribution of small molecules and antiangiogenic proteins following intravitreal and SC injections in human eyes.

**RESULTS.** The model predicts that intravitreally administered molecules are substantially mixed within the vitreous following injection, and that the long-term behavior of the injected drug does not depend on the initial mixing. Ocular pharmacokinetics of different drugs is sensitive to different clearance mechanisms. Effective retinal drug delivery is impacted by RPE permeability. For VEGF antibody, intravitreal injection provides sustained delivery to the retina, whereas SC injection provides more efficient, but short-lived, retinal delivery for smaller-sized molecules. Long-term suppression of neovascularization through SC administration of antiangiogenic drugs necessitates frequent injection or sustained delivery, such as microparticle-based delivery of antiangiogenic peptides.

**CONCLUSIONS.** A comprehensive 3D model for intravitreal and SC drug injection is developed to provide a framework and platform for testing drug delivery routes and sustained delivery devices for new and existing drugs.

**Keywords:** ocular drug delivery, antiangiogenic, pharmacokinetics, computational model, systems pharmacology model

Neovascular or wet age-related macular degeneration (AMD) is one of the leading causes of irreversible blindness, affecting over 1.75 million individuals in the United States alone.<sup>1</sup> The hallmark of AMD is the degeneration of retinal macula and retinal neovascularization. The fragile and leaking new vessels cause a buildup of blood and fluid in the retinal macula, scarring the macular tissues, resulting in a loss of central vision, and eventually leading to irreversible vision loss if left untreated. Studies of the pathophysiology of AMD have suggested that choroidal neovascularization is dynamically controlled by the balance of proangiogenic factors, such as vascular endothelial growth factor (VEGF), and antiangiogenic factors, such as pigment epithelium derived factor (PEDF) in the eyes.<sup>2</sup> The upregulation of VEGF promotes a pathologic state of retinal pigmented epithelium (RPE) that causes choroidal neovascularization.<sup>3</sup> Macular edema (ME), characterized by the buildup of fluid, usually is caused by increased vascular permeability and vascular leakage. A particular type of ME related to diabetes, called diabetic macular edema (DME), results from an increased VEGF level caused by hypoxia response of cells. Current standard of care of AMD and ME mostly involves intravitreal injection of anti-VEGF and anti-

permeability drugs that reduce vascular leakage and neovascularization. Therapeutic agents delivered to the eye through intravitreal injection normally require a monthly or bimonthly treatment. Given that these frequent direct injections into the eye may cause discomfort and adverse effects, alternative strategies for delivering therapeutic drugs to the posterior segment of the eye have been studied and developed. The suprachoroidal space is a potential space between the sclera and choroid in the posterior segment of the eye. When injected, the suprachoroidal (SC) space becomes filled by the injected solution and opens up to approximately 200 to 300  $\mu\text{m}$  of thickness. This technique is less invasive, better targeted to the layers in the back of the eye, and does not cause the injected solution to be diluted by vitreous humor. It provides a promising way of targeted delivery of antiangiogenic therapeutics.<sup>4</sup> The detailed mechanisms and characteristics of this technique, including the thickness and closure kinetics of the SC space following injection, and clearance routes have been studied thoroughly by Chiang et al.<sup>5,6</sup> This minimally-invasive method uses a microneedle to inject drugs to the SC space from which the active agents would diffuse to the surrounding tissues. Recently, SC injection has been studied extensively as a

method of sustained delivery of drugs, such as triamcinolone acetonide (TA).<sup>7,8</sup>

Anti-VEGF therapy for AMD and ME uses intraocular injection of VEGF-neutralizing antibodies, ranibizumab and bevacizumab, or a fusion VEGF receptor aflibercept, that have been shown to provide substantial benefits to patients; however, in a significant percentage of patients these therapeutic interventions are unable to eliminate neovascularization and edema, suggesting that other pathways and factors might be involved.<sup>9,10</sup> Antiangiogenic short peptides are emerging as new promising agents for the treatment of AMD and ME. Classes of antiangiogenic peptides have been discovered;<sup>11</sup> among them a serpin-derived peptide has been shown to be a promising potential therapeutic along with its biodegradable polymeric microparticle-based delivery system.<sup>12</sup> Recently, a collagen IV-derived peptide has been demonstrated in several animal models to significantly reduce neovascularization and vascular leakage.<sup>13</sup> To reduce the frequency of injections and to prolong the action of the antiangiogenic peptides, peptide-containing microparticles that slowly release peptide over an extended period of time can be injected to provide sustained inhibition of neovascularization and vascular leakage. Effective antiangiogenic agents including small molecule tyrosine kinase inhibitors, peptides, antibodies, siRNAs, or genes can be intraocularly delivered as treatment. Considering they can vary significantly in transport properties, characterization of ocular transport of different molecules is especially important to evaluate the efficacy of drug delivery strategies.

Several computational models have been developed for different drug delivery techniques to the posterior segment of the eye including systemic delivery, intravitreal injection, and ocular implants. Balachandran and Barocas<sup>14</sup> used a finite element method (FEM) to simulate the diffusion, convection, and active transport through the diffusion barriers of drugs delivered from systemic source. Jooybar et al.<sup>15</sup> developed a similar model with detailed geometry using FEM-based COMSOL Multiphysics for ocular drug transport following intravitreal injection and ocular implants. Other models focused on in silico investigations of effectiveness of different kinds of ocular implants. Kavousanakis et al.<sup>16</sup> simulated the delivery of an anti-VEGF fragment antibody to the posterior segment of the eye using a polymer gel implant. The pharmacokinetic model developed by Kotha et al.<sup>17</sup> studied a polymer patch-like implant placed on sclera, and the three-dimensional (3D) model developed by Park et al.<sup>18</sup> simulated an implant drug release profile, both using FEM similar to the previous models. Other studies focused on using computational models, in combination with experiments to determine the transport properties of individual components of the eye. For example, Haghjou et al.<sup>19</sup> investigated the outward permeability of different ophthalmic drugs in the retina-choroid-sclera region of the eye, and Ranta et al.<sup>20</sup> analyzed the effect of the diffusion barriers on pharmacokinetics of these ophthalmic drugs. A more recent model developed by Hutton-Smith et al.<sup>21</sup> used a three-compartment model to assess the distribution of intravitreally delivered drugs across the retina, vitreous chamber, and anterior chamber. Despite a plethora of computational models dedicated to study ocular pharmacokinetics of drugs of different classes, there remains a lack of wide comparisons of computational models and experimental data.<sup>22</sup> Recent developments in novel drug delivery techniques, such as SC injection, also warrant anatomically-detailed models of ocular pharmacokinetics validated by experimental data.

We developed a physiologically-based computational 3D model for ocular diffusion of therapeutic drugs following injection into the vitreous cavity and SC space of the eye and

performed simulations using COMSOL Multiphysics software. The model is validated with previously published experimental data for fluorophotometry scans in rabbit eyes following intraocular delivery of molecules of different molecular size including sodium fluorescein (SF), bevacizumab,<sup>4</sup> and ranibizumab.<sup>23</sup> The model then is used to predict the transport of small molecule SF as well as larger antiangiogenic VEGF antibodies following intraocular injection into the human eye. Our model was able to characterize ocular transport of different therapeutic agents across diffusion and permeability barriers in the posterior segment of the eye and compute the local concentration in each layer of the eye to predict the efficacy of different ocular drug delivery strategies for a variety of therapeutic agents.

## METHODS

### Model Geometry

A 3D model detailing anatomical structures of the vitreous and posterior segment of the eye was developed using COMSOL Multiphysics Modeling software (version 5.3; COMSOL, Inc., Burlington, MA, USA). The geometry of the model is shown in Figure 1a. The shape of the eye is assumed to be approximately spherical. This study focused on the transport of the injected species in the posterior segment of the eye only. In this model, the posterior segment was divided into sclera (S), SC space, choroid (C), retina (R), and vitreous (V). The RPE is modeled as a thin layer located between the C and R layers of the eye. The inner limiting membrane (ILM) as a thin layer between R and V separates V from the rest of the posterior segment. Each layer of the posterior segment is represented as a spherical shell. The model geometry and finite-element meshing of the geometry are shown in Figure 2.

### Governing Equations

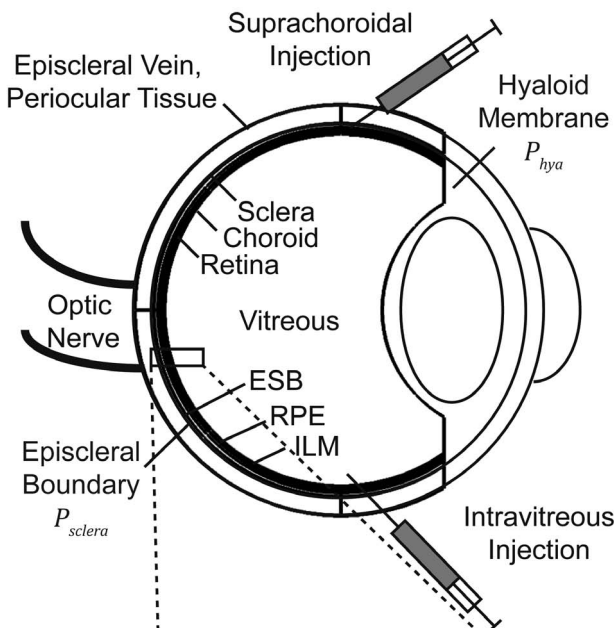
In the model, the five regions of the posterior segment of the eye (S, SC, C, R, and V) have different transport properties as illustrated in Figure 1b. RPE between C and R, and ILM between R and V also are modeled as thin layers that has different transport properties from their adjacent layers. SC is a fluid-filled space created by the injection in the potential space between the sclera and choroid. An aqueous solution containing an experimental or therapeutic molecule or biodegradable particles containing therapeutic molecules is injected into the vitreous or SC space. The general 3D concentration distribution of the molecule is described by the convection-diffusion equation with first order clearance:

$$\phi_j \frac{\partial c}{\partial t} + \nabla \cdot (-D_j \nabla c) + v \cdot \nabla c = -K_{cl,j} c \quad (1)$$

where  $j$  denotes the region in the eye,  $c_j$  is the interstitial concentration,  $\phi_j$  is the void fraction or the fraction of the volume containing the interstitial fluid where the molecules can diffuse freely, as introduced previously,<sup>24</sup>  $D_j$  is the diffusivity,  $v$  is the convective velocity field, and  $K_{cl,j}$  is the clearance rate.

Convection in the back of the eye is driven by the difference in pressure between the hyaloid membrane, anterior to the vitreous humor, and the episcleral vein, posterior to the sclera. Convective flow driven by pressure gradient is modeled as a fluid flow through a porous, incompressible medium, using Darcy's law, as in computational models developed by Balachandran and Barocas<sup>14</sup> and Missel.<sup>25</sup>

**(a) Geometry of the Eye**



**(b) Model Variables**

Permeability	$P_{RPE}$ $P_{ILM}$				
Diffusion Barrier	RPE ILM				
Layer	S	SC	C	R	V
Concentration	$c_s$	$c_{SC}$	$c_C$	$c_R$	$c_V$
Void Fraction	$\phi_s$	$\phi_{SC}$	$\phi_C$	$\phi_R$	$\phi_V$
Diffusivity	$D_s$	$D_{SC}$	$D_C$	$D_R$	$D_V$
Clearance Rate			$K_{Cl,C}$		$K_{Cl,V}$

FIGURE 1. Model diagram showing the geometry of the model. (a) Cross-section of the eye showing layers in the posterior segment of the eye. (b) Layers in the posterior segment and model variables.

$$v = -\frac{K}{\mu} \nabla P \tag{2}$$

where  $\frac{K}{\mu}$  is the hydraulic permeability of the material and  $-\nabla P$  is the pressure gradient. The velocity field  $v$  is proportional to the pressure gradient. Assuming the fluid is incompressible,  $\nabla \cdot v = 0$ , the pressure then can be computed by solving the partial differential equation:

$$\nabla \cdot \left( -\frac{K}{\mu} \nabla P \right) = 0 \tag{3}$$

The velocity field then is calculated from Equation 2. RPE is known to actively transport molecules, such as fluorescein.<sup>26</sup> Active transport is modeled by a constant radially outward convective field in the RPE layer. Rate of active transport of fluorescein is adapted from the model developed by Balachan-

dran and Barocas.<sup>14</sup> No active transport is assumed for antiangiogenic proteins.

**Clearance Mechanisms**

Intraocularly delivered drug clears from the eye through anterior and posterior clearance. In anterior clearance, drug is cleared from the vitreous humor through permeation to the anterior chamber across the hyaloid membrane. Existence of certain enzymes also suggests that a small amount of enzymatic degradation can take place within the vitreous.<sup>22</sup> In posterior clearance, drug is cleared through the choroidal vasculature and episcleral vein. Anterior clearance and loss to choroidal vasculature are modeled with first-order clearance according to the pharmacokinetic model developed by Hutton-Smith et al.<sup>21</sup> Clearance through episcleral vein is modeled with a constant flux boundary condition at the outer surface of sclera according to anatomically-detailed finite element models developed by Balachandran and Barocas<sup>14</sup> and Missel.<sup>25</sup>

**Boundary Conditions and Initial Conditions**

Flux balances and concentration continuities are applied at all internal boundaries, ensuring that mass balance is maintained for the transport across all internal boundaries separating adjacent layers. At the outer boundary of the sclera, a constant flux  $-k_s \cdot c$  is applied to model the loss of drug to the episcleral vein. Zero-flux conditions are applied at all other exterior boundaries.

The injection into the SC space is assumed to be instantaneously mixed within the SC region and is modeled by specifying initial concentration  $c_{0,SC}$  in the SC region. Intravitreal injection is modeled by the assumption that immediately after injection, the injected solution is partially mixed in a subvolume of vitreal fluid and settles at the bottom of the eye due to its higher specific gravity (Campochiaro PA, unpublished observations). Sensitivity to the values of the mixed subvolume is presented below and this parameter is shown not to be important except for short time after injection.

**Parameter Estimation**

All parameters used in the model for rabbit and human eyes are presented in Supplementary Table S1. Scleral permeability in rabbit eyes has been shown to follow an exponential fit to the molecular radius of the molecule as demonstrated in in vitro experiments.<sup>27</sup> Least-square regression was performed on the values reported by the study, and used to predict the permeability for SF, 40 kDa Dextran, 250 kDa Dextran, ranibizumab, and bevacizumab. Diffusion coefficients for these molecules then are estimated by multiplying predicted permeability values by scleral thickness.

Diffusion coefficients of the other layers of the eye then are estimated by the empirical relation between diffusivity and void fraction as described by the following equation.<sup>28</sup>

$$D_j = D_s \frac{\phi_j (3 - \phi_s)}{\phi_s (3 - \phi_j)}$$

where  $\phi_j$ ,  $D_j$  are the void fraction, interstitial volume fraction, and diffusion coefficients of layer  $j$ , and  $\phi_s$ ,  $D_s$  are the void fraction and diffusion coefficients of sclera.

Transport through RPE is characterized by permeability across the thin RPE layer. It has been shown that RPE has lower permeability for molecules of larger size, and that RPE permeability decreases exponentially with respect to the molecular radius.<sup>29</sup> Literature values for in vitro permeabilities

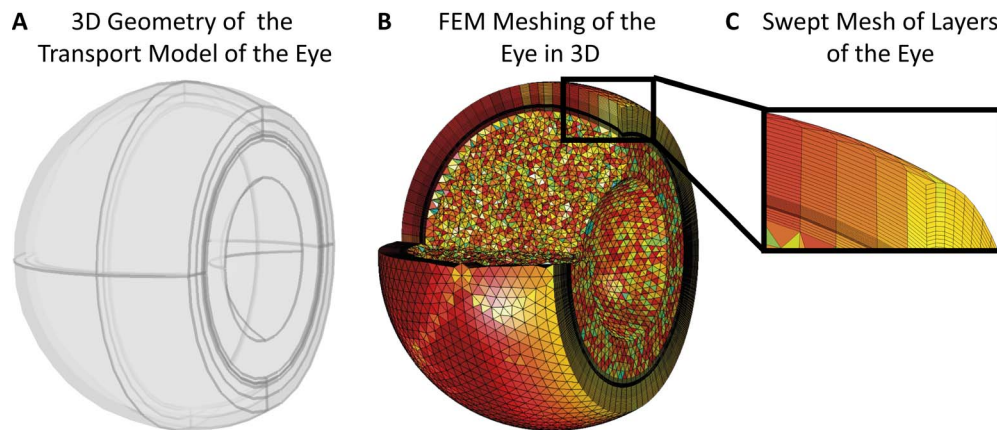


**FIGURE 2.** Finite-element model meshing of the model geometry. (A) 3D geometry of the posterior segment of the eye constructed in COMSOL Multiphysics. (B) Meshing of the eye used for finite element method calculation. (C) Swept meshing of the thin layers in the posterior segment.

of carboxylfluorescein, 4 kDa FITC-Dextran, 10 kDa FITC-Dextran, 20 kDa FITC-Dextran, 40 kDa FITC-Dextran, and 80 kDa FITC-Dextran are fitted exponentially to their Stokes-Einstein radius. Baseline RPE permeability of SF is estimated using the exponential fit and molecular radius. It has been shown that ILM would permit molecules smaller than 70 kDa to diffuse across it.<sup>30</sup> In the present model, ILM is not considered a resistive barrier for small molecules such as SF; for large molecules permeability across ILM is assumed to be lower than its adjacent layers. Estimate of permeabilities of ranibizumab and bevacizumab across ILM and RPE are adapted from an experimentally-validated compartmental model developed by Hutton-Smith et al.<sup>21</sup>

Geometric parameters, including thicknesses and void fractions of layers in human eyes are adapted from Mac Gabhann et al.<sup>24</sup> Dimensions of rabbit eyes, thickness of RPE, and thickness of SC space after injection into SC space are obtained from experimental studies and optical images of posterior segment of rabbit eyes.<sup>4,31</sup> Thickness of ILM is adapted from experimental studies on ILM morphometry.<sup>32</sup> Parameters characterizing convective flow within the eye, including hydraulic resistivities, pressure at hyaloid membrane and sclera are adapted from the study of Balachandran and Barocas.<sup>14</sup> Pressure at hyaloid membrane, the intraocular pressure (IOP), is assumed to rise to 30 mm Hg immediately after injection and reduced stepwise to 15 mm Hg at 30 minutes after injection.<sup>35</sup>

### Initial Distribution of Drug Immediately Following Intracocular Injection

The initial condition is given by specifying the initial distribution of the drug immediately following intracocular injection. For intravitreal injection, the injected fluid is assumed to partially mix within the vitreous and be significantly diluted. Intravitreally administered solutions of fluorescently-labeled ranibizumab have higher specific gravity compared to mostly aqueous vitreous humor that has a density similar to that of water.<sup>34</sup> Therefore, due to the higher specific gravity of the injected fluid, it is further assumed that the mixture settles at the bottom of the vitreous humor; however, we showed that this assumption only affects the concentration distribution at the initial times, with the long-term behavior only dependent on the amount of injected species. Note that the hydrodynamics of mixing for fluids with different viscosities and specific gravities relevant to the problem of intravitreal injection is a complex phenomenon and has not been investigated to our knowledge; however, relevant studies

for a fluid jet impinging on a fluid reservoir suggest that the mixing effect is significant.<sup>35,36</sup> The degree of the initial mixing that occurs following intravitreal injection is explored in more detail in the Results section. We also assume a similar initial distribution for SF solution. For SC delivery, the injected fluid is assumed to immediately fill the SC space homogeneously following injection.

Details of the numerical solution of the above transport equations are presented in Supplementary Materials.

## RESULTS

### Intravitreally Administered Solution is Mixed Significantly in the Vitreous

The degree to which intravitreally administered solution containing SF or fluorescently-labeled ranibizumab is mixed within the vitreous, as well as the long-term impact of the initial distribution were explored *in silico* by varying the volume that the solution initially occupies immediately after injection.

For intravitreal injection of 50  $\mu\text{L}$  aqueous solution containing ranibizumab, the solution was assumed to be mixed with the vitreous humor to form a mixture that settles at the bottom of the vitreous as discussed above. To investigate the degree of mixing, the mixture was assumed to occupy 50  $\mu\text{L}$  (same as injected volume), 250  $\mu\text{L}$  (5 times the injected volume), and 400  $\mu\text{L}$  (8 times the injected volume) in the initial condition. As shown in Figure 3, the concentration distributions at different time points following injection computed with different initial conditions were compared to previously reported experimental fluorophotometry data.<sup>23</sup> The simulation results showed that the assumption of the mixture occupying 400  $\mu\text{L}$  was most consistent with experimental data. In Figure 3C, the concentration along the visual axis shows the greatest difference due to mixing 1 day after injection. Four days after injection and later, the concentration profiles from different degrees of mixing were within 5% of their average, showing that the concentration distribution of injected species was only affected at initial times, and that the long-term behavior only depended on the amount of drug injected. As shown in Figure 3D, the pharmacokinetic profile showing the average concentration of ranibizumab in the vitreous following injection also were independent of the mixing.

Similar results were obtained from the simulation of intravitreal injection of SF. Simulation results with the assumption of the injected mixture occupying 400  $\mu\text{L}$  were most consistent with experimental data (Supplementary Fig. S1).

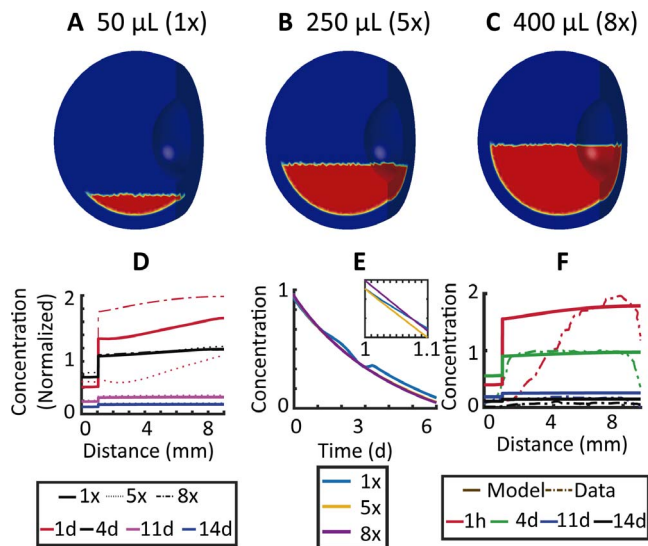


**FIGURE 3.** Initial mixing of intravitreal injection of ranibizumab in rabbit eyes. (A–C) Initial conditions of concentration distribution assuming that the injected solution mixes with the vitreous, occupying (A) 50  $\mu\text{L}$ , (B) 250  $\mu\text{L}$ , and (C) 400  $\mu\text{L}$  of volume. (D) Predicted concentration along visual axis 1, 4, 11, and 14 days following injection under the assumption that the injected solution mixes with the vitreous, occupying 50  $\mu\text{L}$  (solid), 250  $\mu\text{L}$  (dotted), and 400  $\mu\text{L}$  (dashed) of volume. (E) Model prediction of average concentration in vitreous over time under different initial conditions of mixing. (F) Comparison of model prediction of concentration along the visual axis under the assumption that the initial mixture occupies 400  $\mu\text{L}$  of volume and experimental fluorophotometry data.

### Fitting of Clearance Rates to Experimental Data

The clearance rates of intraocularly-administered SF, ranibizumab and bevacizumab were fitted to experimentally measured pharmacokinetic profiles.<sup>4,23</sup> To fit the model to the pharmacokinetic profiles, model sensitivity to parameters characterizing drug clearance (clearance rate in choroid and vitreous  $k_{cl,c}$ ,  $k_{cl,v}$ , as well as scleral loss rate  $k_s$ ) following intraocular injection was assessed. For intravitreally delivered sodium fluorescein and ranibizumab, vitreous concentration following injection was only sensitive to clearance rate in vitreous (Supplementary Figs. S2A, S2C). Concentration of suprachoroidally injected sodium fluorescein in the SC space was sensitive to scleral loss rate  $k_s$  (Supplementary Fig. S2B), while concentration of suprachoroidally injected bevacizumab in the SC space was sensitive to choroidal clearance rate  $k_{cl,c}$  (Supplementary Fig. S2D). The sensitive parameters then were fitted to the experimental data. Representative pharmacokinetic profiles using different values for clearance parameters of SF transport following intravitreal and SC injection, ranibizumab transport following intravitreal injection, and bevacizumab transport following SC injection, along with experimental data are shown in Figures 4e to 4h. Fitted clearance rates then were used for 3D simulation of transport following intraocular injection in human eyes.

### Intraocular Administration of Sodium Fluorescein in Rabbit Eyes: Comparison With Experimental Data

Concentration of SF along the visual axis as predicted by the model was compared to the published fluorophotometry measurements for validation<sup>4</sup> (Figs. 4a, 4b). 3D concentration distributions of SF at different time points following injection

are shown in Supplementary Figure S3. The experiment and simulation show that SF cleared from the eye faster following SC injection. Following intravitreal injection, concentration of SF reached 10% of peak concentration approximately 7 hours after injection, and 90% cleared out 6 hours after injection, whereas following SC injection, SF reached 20% of the peak concentration approximately an hour after injection and 95% cleared out approximately 6 hours after injection, much faster than intravitreally administered SF.

### Intraocular Administration of Antiangiogenic Proteins

Simulations of transport in the rabbit eyes of ranibizumab following intravitreal injection and bevacizumab following SC injection were performed using the model. Concentration profiles along the visual axis at different time points following injection were compared to fluorophotometry scans for validation (Figs. 4c, 4d).<sup>23</sup> 3D concentration distributions of ranibizumab and bevacizumab at different time points following injection are shown in Figure 5. The simulation and experiment showed that ranibizumab was distributed homogeneously within the vitreous approximately two days following injection and that 90% of ranibizumab cleared from the vitreous 14 days following injection. For SC injection of bevacizumab (Figs. 4d, 4h), bevacizumab was concentrated mostly near the SC space, and 90% of bevacizumab cleared out 12 hours after injection.

### Simulation of Intraocular Administration of Sodium Fluorescein and Antiangiogenic Proteins Into Human Eyes

The model was adjusted to human eye dimensions for prediction of transport of SF in human eyes following intravitreal and SC administration. Transport of molecules of similar size to SF, such as small molecules or short therapeutic peptides, following intraocular injection should be similar to that of SF, unless their distributions are affected by binding to their target receptors; simulations for therapeutic peptides using similar models will be presented elsewhere. Prediction of concentration distributions of SF in human eyes following intravitreal injection and SC injection is presented in Figure 6. For intravitreally administered SF (Figs. 6a–c), the injected solution was significantly diluted in the vitreous. Retinal concentration was similar to the vitreal concentration. Choroidal and scleral concentrations were lower than the concentration in retina. Vitreal concentration of SF was at 20% of its peak value approximately 6 hours after injection and 90% of the injected SF cleared out from human eyes approximately 10 hours after injection. For SC injection of SF (Figs. 6d–6f), the injected solution was held at the SC space between sclera and choroid. The fluid was not diluted and the concentration of SF in the SC space was similar to the concentration of the injected fluid. The choroidal concentration was similar to the concentration in the SC space. Retinal concentration closely followed SC concentration starting from approximately 2 hours after injection. Significantly less SF diffused into the vitreous. Scleral concentration of SF was at approximately 20% of its maximum value 24 hours after injection.

The model also was used to predict transport of anti-VEGF antibodies following intraocular administration, including intravitreally-administered ranibizumab and suprachoroidally-administered bevacizumab in human eyes. Concentration distributions in human eyes following intraocular injection are shown in Figure 7. Transport of ranibizumab and bevacizumab represented the transport of similarly-sized

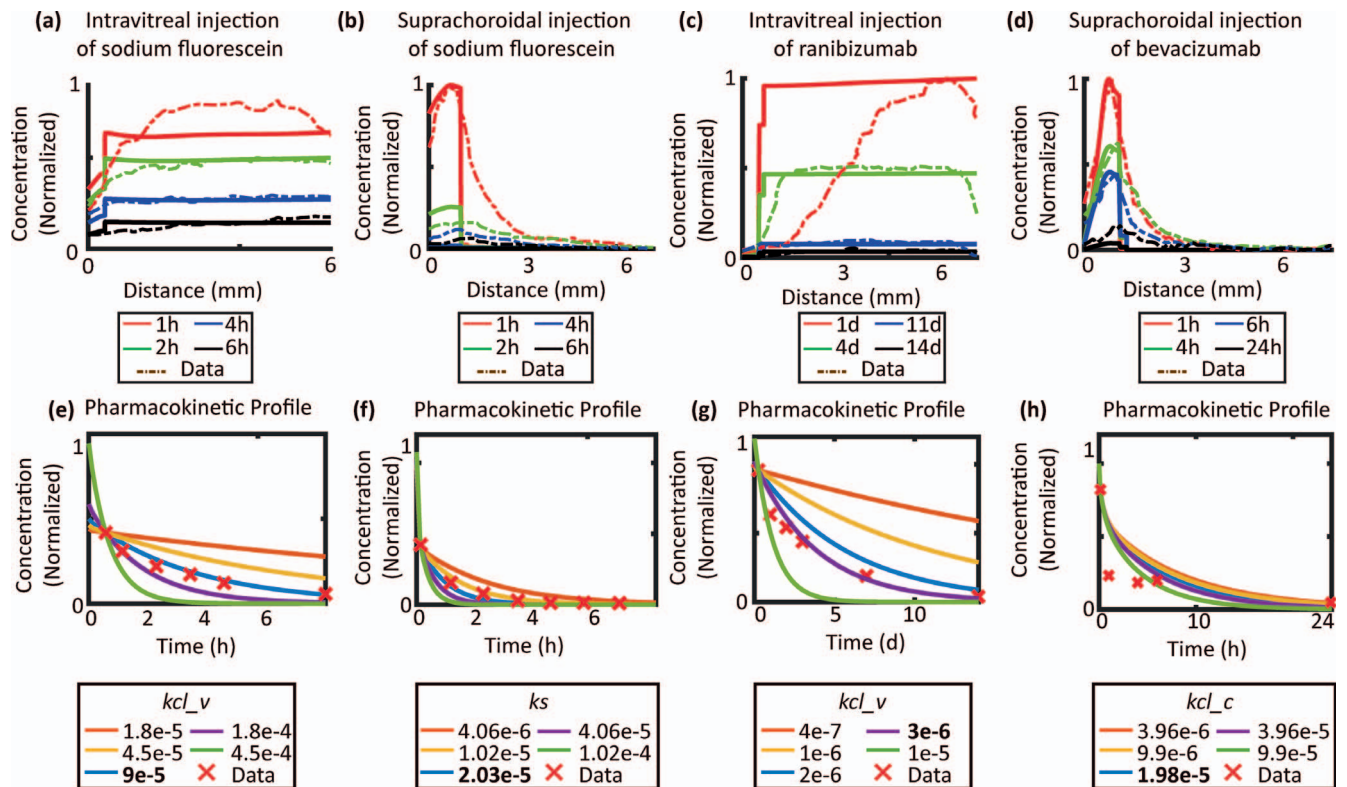


**FIGURE 4.** Model simulation and data validation of transport of molecules following intraocular administration in rabbit eyes. (a–d) Model prediction of concentration along the visual axis following (a) intravitreal injection of SF, (b) suprachoroidal injection of SF, (c) intravitreal injection of ranibizumab, and (d) SC injection of bevacizumab at different time points following injection compared to experimentally measured fluorophotometry data. (e–h) Fitting of clearance rates of (e) intravitreal injection of SF, (f) SC injection of SF, (g) intravitreal injection of ranibizumab, and (h) SC injection of bevacizumab.

antiangiogenic proteins following intraocular administration. As with SF, intravitreally administered ranibizumab was significantly diluted in the vitreous following intravitreal injection. As shown in Figure 7c, retinal concentration was similar to vitreal concentration. The scleral and choroidal concentrations were significantly lower. Suprachoroidally-injected bevacizumab was not diluted, and targeted directly the chorioretinal tissues. Following SC administration (Fig. 7d), bevacizumab concentrations in the SC space and choroid were at the same level, and retinal concentration was significantly lower due to the permeation-limiting RPE. It should be noted that, while after intravitreal administration the level of the drug persisted for over 2 weeks, after SC administration the drug persisted on the order of a day, which should necessitate either frequent injections, which is not practical, or the use of sustained delivery, such as microparticle-based delivery.

### Parameter Sensitivity for RPE and ILM Permeability

Retinal delivery of antiangiogenic proteins is affected by the diffusion barrier RPE between choroid and retina, and by the diffusion barrier ILM between retina and vitreous. Permeability of molecules across these barriers can vary between individuals, and some diseases would cause structural changes of the RPE and ILM; therefore, varying their transport properties as discussed below. The data used for model validation were not spatially resolved enough to accurately assess the permeability across the thin diffusion barriers, due to the nature of the fluorophotometry experiments. Therefore, the uncertainty due to RPE and

ILM permeability was explored by comparing the results obtained from varying the RPE and ILM permeabilities from their baseline values (Fig. 8).

For intravitreal injection, ILM resists drug entrance into the retina from the vitreous, while RPE keeps drug from leaving the retina to the choroid where it is lost to circulation. Vitreal concentration is not sensitive to RPE and ILM permeability (Figs. 8a, 8c). Retinal concentration is very sensitive to RPE permeability, but not to ILM permeability (Figs. 8b, 8d). A 5-fold increase in RPE permeability causes peak retinal concentration to decrease by more than 60%.

For SC delivery, RPE is the diffusion barrier that keeps injected molecules from entering the retina. Figures 8e to 8h show the SC and retinal concentrations following SC administration of bevacizumab using different RPE and ILM permeability values. Retinal concentration of bevacizumab showed high sensitivity to RPE permeability (Fig. 8f) and low sensitivity to ILM permeability (Fig. 8h). A 5-fold increase in RPE permeability resulted in an approximately 6-fold increase in peak retinal concentration.

## DISCUSSION

### Intravitreally Administered Solutions are Partially Mixed Within the Vitreous Humor Immediately After Injection

For intravitreal injection of a solution containing certain substances, assuming the injected fluid is less viscous than

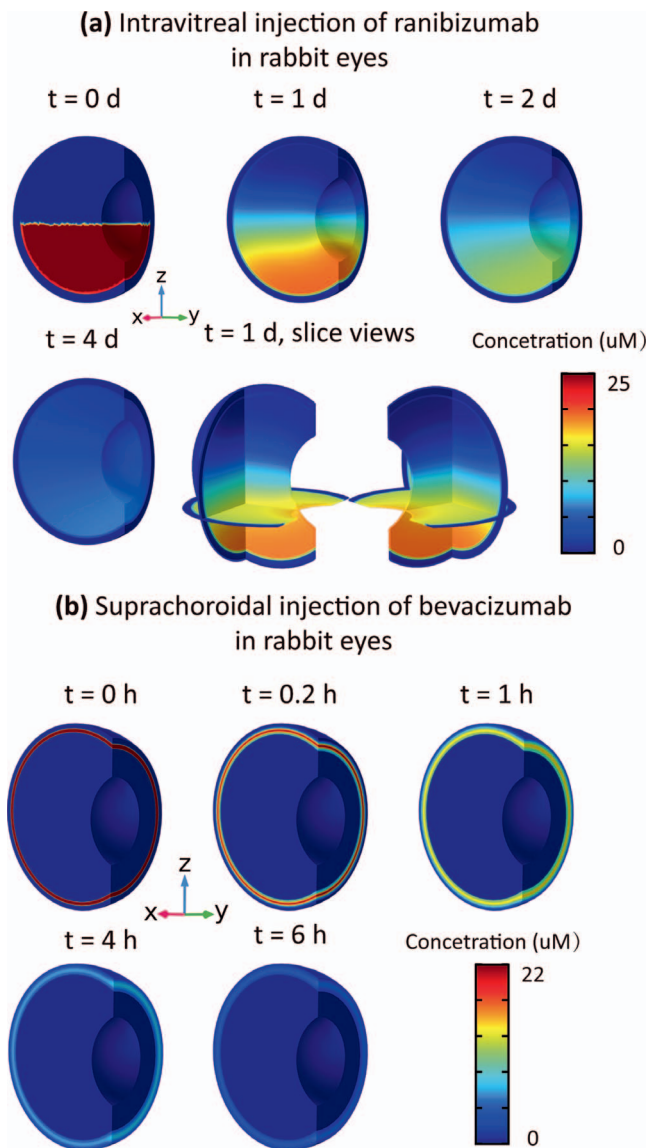


**FIGURE 5.** 3D distribution of ranibizumab and bevacizumab concentration following intraocular administration in rabbit eyes. (a) Concentration distribution at 0, 1, 2, 4, and 6 days following intravitreal injection of ranibizumab. (b) Concentration distribution at 0, 0.25, 0.5, 1 and 4 hours following SC injection of bevacizumab.

the vitreous humor (the relative viscosity of vitreous humor has been reported as 1.59)<sup>37</sup> and the injection of approximately 50  $\mu$ L liquid is performed using a 28-gauge (G) or similar needle within one second, the Reynolds number is estimated to be approximately 350. Based on an experimental study of a submerged fluid jet injected into a reservoir, with the same or different viscosities,<sup>35,36</sup> significant mixing would occur during the injection process. The viscosity of the human vitreous depends on many factors, such as age and disease. Relative viscosity of human vitreous varies from approximately 1 at birth to over 2 at later age.<sup>37</sup> Vitreous viscosity also can be affected by conditions, such as myopia, and ocular procedures, such as cataract extraction.<sup>37,38</sup> Additionally, different injection speed or needle size would affect the Reynolds number of the injected solution, and result in different initial distribution of the drug immediately after injection. Therefore, significant mixing of injected solution and vitreous humor would occur immediately following intravitreal injection. Mixing causes the

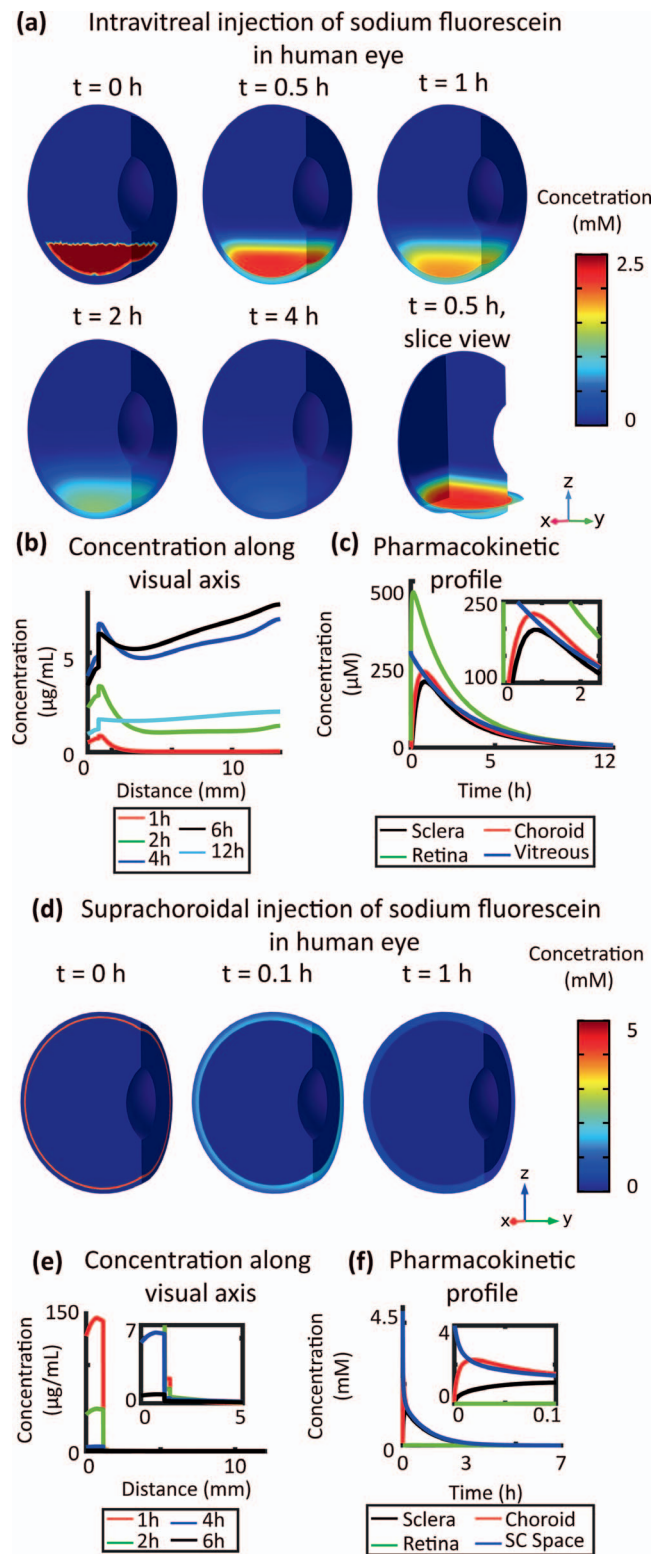


**FIGURE 6.** Model prediction of SF transport in human eyes following (a–c) intravitreal injection, and (d–f) SC injection. (a) Predicted 3D concentration distribution at 0, 1, 2, 4, and 6 hours following intravitreal injection. (b) Predicted concentration along the visual axis 1, 2, 4, 6, 12, and 24 hours following intravitreal injection. (c) Average concentration over time in sclera, choroid, retina, and vitreous following intravitreal injection. (d) Predicted 3D concentration distribution at 0, 0.5, and 1 hour following SC injection. (e) Predicted concentration along the visual axis at 1, 2, 4, 6, 12, and 24 hours following SC injection. (f) Average concentration over time in sclera, choroid, retina, and SC space following intravitreal injection.

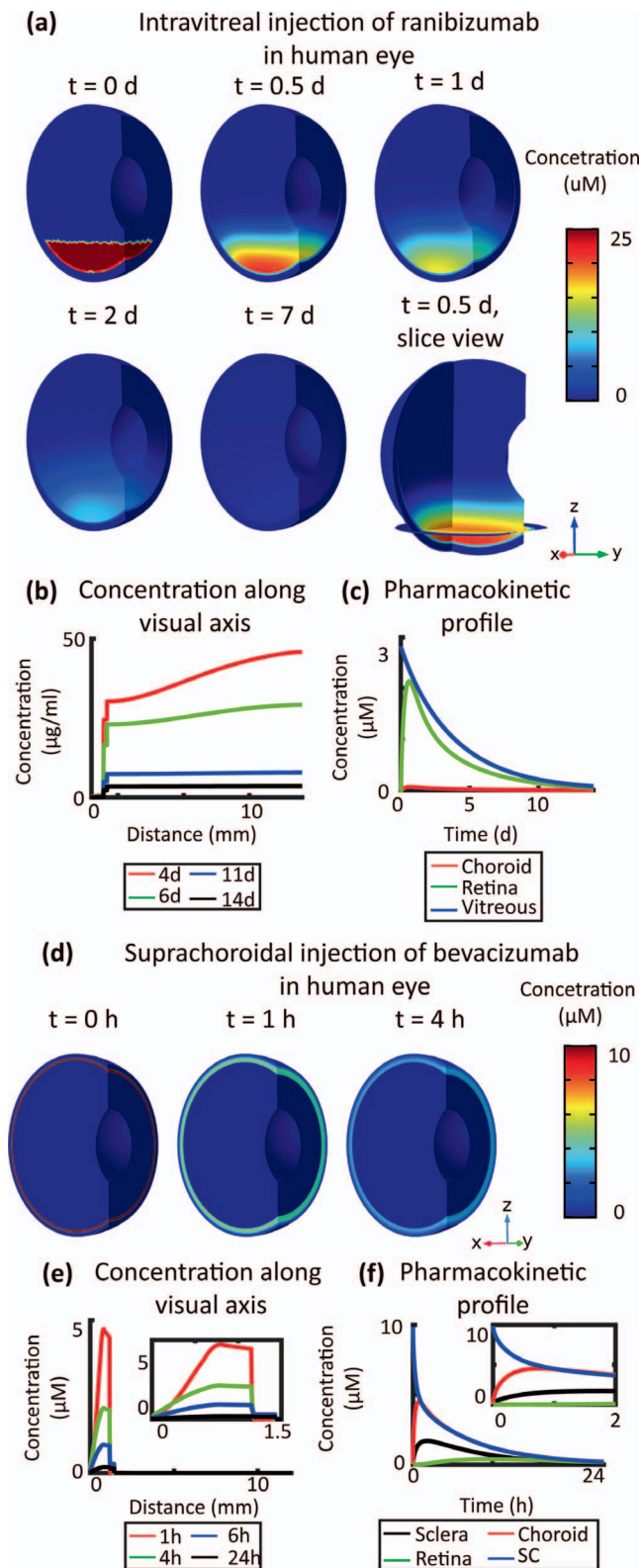


**FIGURE 7.** Model prediction transport in human eyes following (a–c) intravitreal injection of ranibizumab, and (d–f) SC injection of bevacizumab. (a) Predicted 3D concentration distribution of ranibizumab at 0, 1, 2, 4, and 7 days following intravitreal injection. (b) Predicted concentration of ranibizumab along the visual axis 1, 2, 4, 7, 11, and 14 days following intravitreal injection. (c) Average concentration over time in sclera, choroid, retina, and vitreous following intravitreal injection of ranibizumab. (d) Predicted 3D concentration

injected solution to be diluted and to occupy 2 to 10 times the injected volume within the vitreous. The degree to which the mixing occurs is likely to vary among individuals due to all of the aforementioned reasons.

However, as demonstrated in the Results, the long-term distribution of drug concentration after the administered drug has reached homogeneity within the vitreous is less impacted by the initial distribution, and therefore, would less likely be affected by this individual variability and would show more consistency among individuals.

### Routes of Clearance Following Intraocular Injection Depend on Method Of Delivery and Molecule Size

Sensitivity to clearance parameters demonstrated in Supplementary Figure S2 showed that for intravitreally delivered drugs, the pharmacokinetic profiles of the drug in vitreous and retina are most sensitive to clearance rate in vitreous. For suprachoroidally-delivered drugs, however, choroidal clearance and episcleral clearance can have a role. For small molecules, such as fluorescein, the concentration profile is most sensitive to clearance from the episcleral vein. For large molecules, such as bevacizumab, the concentration profile in the SC space and retina is insensitive to episcleral clearance rate, but sensitive to choroidal clearance rate. This suggests that molecular size and delivery method can affect the clearance routes. Small molecules that diffuse more readily to the episcleral surface will become cleared into the circulation through the episcleral vein. Large molecules will be cleared primarily through choroidal vasculature. Design of an optimal drug delivery strategy must consider contributions of different clearance routes and any conditions that might affect them (for example, high IOP can limit the clearance through the anterior routes and high vein pressure can limit posterior clearance).

### Effectiveness of Retinal Delivery of Drugs can be Affected by RPE and ILM Permeability

The model demonstrated that effectiveness of retinal delivery of large-sized molecules is sensitive to RPE and ILM permeability. Retinal delivery from the intravitreal route was mostly affected by RPE permeability, and retinal delivery from the SC route was affected by RPE and ILM. RPE permeability is known to have high individual variability due to age and diseases. Thus, diseases that cause the structural changes to RPE, such as diabetic retinopathy, would alter the effectiveness of retinal delivery through SC or intravitreal injection. For individuals with diseases that cause the RPE barrier permeability to be significantly higher, for example, targeted delivery of drug to the retina would be more easily achieved through SC injection because RPE no longer limits the permeation of drug from choroid to retina.

In vivo fluorophotometry is a powerful tool for studying the pharmacokinetics of intraocularly administered drugs. However, due to its limited spatial resolution (of 0.25–0.5 mm), and the fact that fluorescence signals are spatially convoluted,<sup>39</sup> further limiting its accuracy in evaluating the concentration gradient along the visual axis, fluorophotometry data are not sufficient in quantitative studies of the transport property of RPE as a diffusion barrier.

distribution of bevacizumab at 0, 1, 2, 4, and 6 hours following SC injection. (e) Predicted concentration of bevacizumab along the visual axis 1, 2, 4, 6, 12, and 24 hours following SC injection. (f) Average concentration over time in sclera, choroid, retina, and SC space following intravitreal injection of bevacizumab.

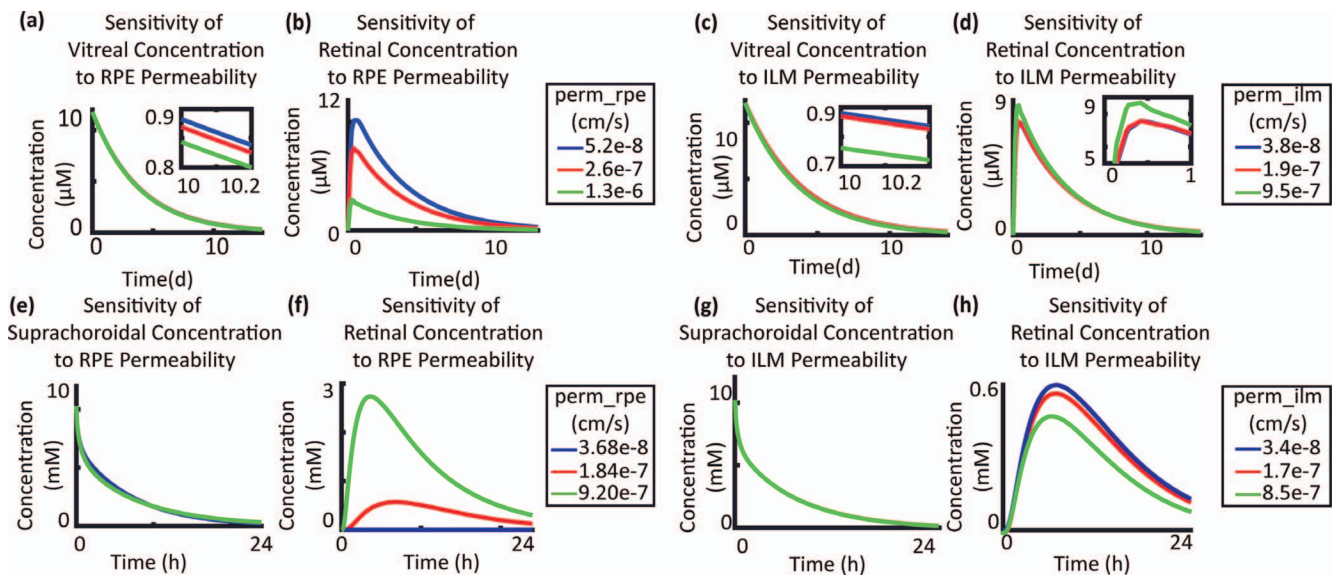


**FIGURE 8.** Sensitivity of ranibizumab transport to (a, b) RPE permeability and (c, d) ILM permeability following intravitreal injection into rabbit eyes, and sensitivity of bevacizumab transport to (e, f) RPE permeability and (g, h) ILM permeability following SC injection into rabbit eyes (a) Vitreal concentration and (b) retinal concentration of ranibizumab over time following intravitreal injection in rabbit eye predicted by the model using RPE permeability being one-fifth of the baseline value, the baseline value, and five times the baseline value. (c) Vitreal concentration and (d) retinal concentration of ranibizumab over time following intravitreal injection in rabbit eye predicted by the model using ILM permeability being one-fifth of the baseline value, the baseline value, and five times the baseline value. (e) SC concentration and (f) retinal concentration of bevacizumab over time following SC injection in rabbit eye predicted by the model using RPE permeability being one-fifth of the baseline value, the baseline value, and five times the baseline value. (g) SC concentration and (h) retinal concentration of bevacizumab over time following SC injection in rabbit eye predicted by the model using ILM permeability being one-fifth of the baseline value, the baseline value, and five times the baseline value.

### Drug Delivery to the Retina Following SC Injection is Sensitive to Permeability Across the RPE

Although concentration in the SC space following SC injection of bevacizumab is sensitive to choroidal clearance rate and largely unaffected by permeability across diffusion barriers (Supplementary Fig. S4A), retinal concentration is very sensitive to permeability across RPE compared to clearance parameters. The model predicted that a 5-fold decrease in permeability prevents most of the drug from entering the retina following SC injection of bevacizumab (Supplementary Fig. S4B).

### Molecules of Smaller Size Can Permeate Through the Diffusion Barrier and Reach Retina More Easily

In the simulations and experiments on intraocular drug delivery in human and rabbit eyes, SF and antiangiogenic proteins represent molecules of small and large hydraulic radii, respectively. The effectiveness of delivery of antiangiogenic agents to the retina through intraocular injection is limited due to the existence of permeation-limiting barriers, such as RPE and ILM. For transscleral administration of antiangiogenic drugs, the molecules must pass through an additional barrier, the episcleral boundary (ESB). Although the transport properties of ESB as diffusion barriers are not as well understood and characterized, all the diffusion barriers, ESB, RPE, and ILM, are likely to limit the diffusion of larger size molecules. The model predicts that SF reaches retina more easily than large antiangiogenic proteins, such as ranibizumab, because the permeation-limiting effect is significantly lower for smaller compared to larger-sized molecules. Thus, for effective retinal delivery of antiangiogenic agents for suppression of angiogenesis, drugs of smaller molecular radius, such as short peptides with antiangiogenic properties, are more desirable due to better permeation through the diffusion barriers. Drugs of smaller molecular radius, however, have a shorter half-life

compared to large antiangiogenic proteins, like ranibizumab and bevacizumab. Therefore, achieving a sustained suppression of neovascularization would necessitate some form of sustained delivery, such as a microparticle-based delivery system that encapsulates nanoparticles formulated with a therapeutic peptide;<sup>12</sup> in addition, a therapeutic peptide has been shown to form a natural depot upon injection and that is slowly released from the depot.<sup>12,13</sup>

### Intravitreal Injection of Antiangiogenic Proteins Provides More Sustained Suppression of Angiogenesis

Intravitreally administered molecules remain largely inside the vitreous humor following injection. The benefit of intravitreal compared to SC injection for delivery of antiangiogenic proteins is more sustained suppression of angiogenesis. For intravitreal injection of ranibizumab in rabbit eyes, for example, ranibizumab is present for as long as 14 days following injection. Drugs administered through the SC space show faster clearance following injection. Suprachoroidally administered bevacizumab cleared out 90% 6 hours following injection. This limitation can be overcome by using some form of sustained delivery, such as ocular implants, microparticle-based drug delivery systems, or depot formation by some antiangiogenic peptides.

### SC Administration Provides More Efficient Retinal Delivery for Smaller Molecules and Clearance is Faster Following Injection

Intravitreally administered drug formulation is significantly mixed and diluted inside the vitreous humor. This would mean that to achieve similar concentration, a larger dose would be needed for intravitreal administration compared to SC injection.

tion. However, the invasiveness of intravitreal injection makes this intraocular drug delivery route less desirable. Intravitreal injection is associated with rare complications, such as retinal detachment and cataract. SC injection, as a less invasive alternative to intravitreal injection, uses a microneedle to inject directly between the choroid and retina in the back of the eye, avoiding injection directly into the eye altogether. As discussed previously, during SC injection, the SC space will open up gradually while becoming filled with the injected solution. This would mean almost no dilution occurs during SC administration of drugs. The SC space simply holds the injected fluid and serves as a reservoir for diffusion of drug into the choroid and retina. Following SC delivery, as predicted by the model, the drug concentrates near the SC space, and stays mostly near the scleral, choroidal, and retinal tissues. For large molecules, such as many antiangiogenic proteins, including bevacizumab and ranibizumab, however, the effectiveness of retinal delivery through SC injection is limited due to the permeability-limiting RPE between choroid and retina that keeps large molecules from entering the retina from the choroid. This could be overcome by using smaller molecules, such as short antiangiogenic peptides, as small molecules can move much more freely across the RPE. We proposed that using a combination of the SC injection technique to reduce invasiveness, drugs of small molecular size to better permeate through the RPE, and sustained delivery systems, such as a natural depot formation or biodegradable microparticles, would achieve sustained suppression of neovascularization with benefits to patients of wet AMD and ME.

### Limitations of the Model

The model does not consider binding of the drugs to the tissues within the eye. Although permeability values used in the model are measured in ocular tissue, drugs can have different binding kinetics in vivo, especially in pathologic conditions where binding can have a major effect on diffusion of the drug and permeation of drug across barriers. In addition, following SC injection, closure kinetics of the SC space and clearance kinetics and clearance routes have been studied. The SC space is observed to close within an hour after injection.<sup>5,6</sup> If the injected fluid in the SC space were squeezed out to the periphery as the SC space closes, the transit of drug concentration in the retina would be further accelerated as a result.

### CONCLUSIONS

We developed a physiologically-based anatomically-correct 3D transport model for intraocular drug delivery. To the best of our knowledge, our model is the first to use spatial concentration distribution from published in vivo fluorophotometry data for validation for a small molecule and a protein drug following intravitreal and SC injections. This provided more confidence in predicting local concentration distribution, which is relevant in many applications including drug delivery to the SC space, placement of ocular implant, and design of optimal delivery strategy for sustained delivery. Our model was fitted to experimental pharmacokinetics data for intravitreally- and suprachoroidally-delivered sodium fluorescein and therapeutic antibody, and validated with in vivo fluorophotometry data. The model was able to predict in rabbit and human eyes the 3D distribution of drugs of different size following intraocular administration.

The model suggested that that the initial mixing effect of the intravitreally-injected drug due to injection has little effect on long-term drug distribution. Distinct clearance mechanisms

differentially impact clearance of drugs of various sizes administered through different routes, and permeabilities of different diffusion barriers will differentially impact effectiveness of intravitreal and SC drug delivery to the retina. The model provided a framework and platform for testing new drugs and sustained delivery devices as well as of regimens for existing ones.

### Acknowledgments

Supported by National Institutes of Health (NIH; Bethesda, MD, USA) Grants 1R21EY026148 and 1R21EY022986, and the Edward N. and Della L. Thome Memorial Foundation.

Disclosure: **Y. Zhang**, None; **H. Bazzazi**, None; **R. Lima e Silva**, None; **N.B. Pandey**, None; **J.J. Green**, None; **P.A. Campochiaro**, Asclepix Therapeutics, LLC (C), Aerpio Therapeutics (C), Alimera (C), Applied Genetic Technologies (C), Genentech/Roche (C), Graybug (C), Regeneron (C), Allegro (C), Intrexon (C), Regenxbio (C); **A.S. Popel**, None

### References

1. Bressler NM. Age-related macular degeneration is the leading cause of blindness. *JAMA*. 2004;291:1900-1901.
2. Campochiaro PA. Molecular pathogenesis of retinal and choroidal vascular diseases. *Prog Retin Eye Res*. 2015;49:67-81.
3. Ohno-Matsui K, Morita I, Tombran-Tink J, et al. Novel mechanism for age-related macular degeneration: an equilibrium shift between the angiogenesis factors VEGF and PEDF. *J Cell Physiol*. 2001;189:323-333.
4. Patel SR, Berezovsky DE, McCarey BE, Zarnitsyn V, Edelhauser HF, Prausnitz MR. Targeted administration into the suprachoroidal space using a microneedle for drug delivery to the posterior segment of the eye. *Invest Ophthalmol Vis Sci*. 2012;53:4433-4441.
5. Chiang B, Wang K, Ethier CR, Prausnitz MR. Clearance kinetics and clearance routes of molecules from the suprachoroidal space after microneedle injection. *Invest Ophthalmol Vis Sci*. 2017;58:545-554.
6. Chiang B, Venugopal N, Grossniklaus HE, Jung JH, Edelhauser HF, Prausnitz MR. Thickness and closure kinetics of the suprachoroidal space following microneedle injection of liquid formulations. *Invest Ophthalmol Vis Sci*. 2017;58:555-564.
7. Chen M, Li X, Liu J, Han Y, Cheng L. Safety and pharmacodynamics of suprachoroidal injection of triamcinolone acetonide as a controlled ocular drug release model. *J Control Release*. 2015;203:109-117.
8. Willoughby AS, Vuong VS, Cunefare D, et al. Choroidal changes after suprachoroidal injection of triamcinolone acetonide in eyes with macular edema secondary to retinal vein occlusion. *Am J Ophthalmol*. 2018;186:144-151.
9. Ferrara N, Damico L, Shams N, Lowman H, Kim R. Development of ranibizumab, an anti-vascular endothelial growth factor antigen binding fragment, as therapy for neovascular age-related macular degeneration. *Retina*. 2006;26:859-870.
10. Spaide RF, Laud K, Fine HF, et al. Intravitreal bevacizumab treatment of choroidal neovascularization secondary to age-related macular degeneration. *Retina*. 2006;26:383-390.
11. Karagiannis ED, Popel AS. A systematic methodology for proteome-wide identification of peptides inhibiting the proliferation and migration of endothelial cells. *Proc Natl Acad Sci U S A*. 2008;105:13775-13780.
12. Shmueli RB, Ohnaka M, Miki A, et al. Long-term suppression of ocular neovascularization by intraocular injection of

- biodegradable polymeric particles containing a serpin-derived peptide. *Biomaterials*. 2013;34:7544-7551.
13. Lima e Silva R, Kanan Y, Miranda AC, et al. Tyrosine kinase blocking collagen IV-derived peptide suppresses ocular neovascularization and vascular leakage. *Sci Transl Med*. 2017;9:eaai8030.
  14. Balachandran RK, Barocas VH. Computer modeling of drug delivery to the posterior eye: effect of active transport and loss to choroidal blood flow. *Pharm Res*. 2008;25:2685-2696.
  15. Jooybar E, Abdekhodaie MJ, Farhadi F, Cheng YL. Computational modeling of drug distribution in the posterior segment of the eye: effects of device variables and positions. *Math Biosci*. 2014;255:11-20.
  16. Kavousanakis ME, Kalogeropoulos NG, Hatzivramidis DT. Computational modeling of drug delivery to the posterior eye. *Chem Eng Sci*. 2014;108:203-212.
  17. Kotha S, Murtomaki L. Virtual pharmacokinetic model of human eye. *Math Biosci*. 2014;253:11-18.
  18. Park J, Bungay PM, Lutz RJ, et al. Evaluation of coupled convective-diffusive transport of drugs administered by intravitreal injection and controlled release implant. *J Control Release*. 2005;105:279-295.
  19. Haghjou N, Abdekhodaie MJ, Cheng YL. Retina-choroid-sclera permeability for ophthalmic drugs in the vitreous to blood direction: quantitative assessment. *Pharm Res*. 2013;30:41-59.
  20. Ranta VP, Mannermaa E, Lummeppo K, et al. Barrier analysis of periocular drug delivery to the posterior segment. *J Control Release*. 2010;148:42-48.
  21. Hutton-Smith LA, Gaffney EA, Byrne HM, Maini PK, Gadkar K, Mazer NA. Ocular pharmacokinetics of therapeutic antibodies given by intravitreal injection: estimation of retinal permeabilities using a 3-compartment semi-mechanistic model. *Mol Pharm*. 2017;14:2690-2696.
  22. Del Amo EM, Rimpela AK, Heikkinen E, et al. Pharmacokinetic aspects of retinal drug delivery. *Prog Retin Eye Res*. 2017;57:134-185.
  23. Dickmann LJ, Yip V, Li C, et al. Evaluation of fluorophotometry to assess the vitreal pharmacokinetics of protein therapeutics. *Invest Ophthalmol Vis Sci*. 2015;56:6991-6999.
  24. Mac Gabhann F, Demetriades AM, Deering T, et al. Protein transport to choroid and retina following periocular injection: theoretical and experimental study. *Ann Biomed Eng*. 2007;35:615-630.
  25. Missel PJ. Simulating intravitreal injections in anatomically accurate models for rabbit, monkey, and human eyes. *Pharm Res*. 2012;29:3251-3272.
  26. Tsuboi S, Pederson JE. Permeability of the isolated dog retinal pigment epithelium to carboxyfluorescein. *Invest Ophthalmol Vis Sci*. 1986;27:1767-1770.
  27. Ambati J, Canakis CS, Miller JW, et al. Diffusion of high molecular weight compounds through sclera. *Invest Ophthalmol Vis Sci*. 2000;41:1181-1185.
  28. el-Kareh AW, Braunstein SL, Secomb TW. Effect of cell arrangement and interstitial volume fraction on the diffusivity of monoclonal antibodies in tissue. *Biophys J*. 1993;64:1638-1646.
  29. Pitkanen L, Ranta VP, Moilanen H, Urtti A. Permeability of retinal pigment epithelium: effects of permeant molecular weight and lipophilicity. *Invest Ophthalmol Vis Sci*. 2005;46:641-646.
  30. Kamei M, Misono K, Lewis H. A study of the ability of tissue plasminogen activator to diffuse into the subretinal space after intravitreal injection in rabbits. *Am J Ophthalmol*. 1999;128:739-746.
  31. Bozkir G, Bozkir M, Dogan H, Aycan K, Guler B. Measurements of axial length and radius of corneal curvature in the rabbit eye. *Acta Med Okayama*. 1997;51:9-11.
  32. Kalvoda J, Duskova J, Kubena A, Povysil C, Kalvodova B. Morphometry of surgically removed internal limiting membrane during vitrectomy in diabetic macular edema. *Graefes Arch Clin Exp Ophthalmol*. 2009;247:1307-1314.
  33. Falkenstein IA, Cheng L, Freeman WR. Changes of intraocular pressure after intravitreal injection of bevacizumab (avastin). *Retina*. 2007;27:1044-1047.
  34. Su X, Vesco C, Fleming J, Choh V. Density of ocular components of the bovine eye. *Optom Vis Sci*. 2009;86:1187-1195.
  35. Cabaleiro JM, Laborde C, Artana G. Interaction between a laminar starting immersed micro-jet and a parallel wall. *Phys Fluids*. 2015;27:013601.
  36. Damian IR, Marculescu C, Balan C. Experiments and Numerical Simulations of Vortex Ring Formation in Microgeometries. *Int Symp Adv Topics Elect Eng (Atee)*. 2015;585-590.
  37. Berman ER, Michaelson IC. The chemical composition of the human vitreous body as related to age and myopia. *Exp Eye Res*. 1964;3:9-15.
  38. Neal RE, Bettelheim FA, Lin C, Winn KC, Garland DL, Zigler JS Jr. Alterations in human vitreous humour following cataract extraction. *Exp Eye Res*. 2005;80:337-347.
  39. Smith RT, Koester CJ, Campbell CJ. Vitreous fluorophotometer data analysis by deconvolution. *Invest Ophthalmol Vis Sci*. 1986;27:406-414.